Multi-functional intelligent drug-loaded microalgae for the repair of diabetic wound: oxygen supply, cell proliferation promotion, and hypoglycemic effect

Shuming Ye[a‡], Neng Jin[ab‡], Yuxin Xu[c‡], Liang Hu[a], Changming Guo[a], Xuehua Jiao[c*], Guiyang Zhang[b*], Juehua Jing[a*]

[a] Department of Orthopaedics, The Second Affiliated Hospital of Anhui Medical University, Hefei 230601, China

[b] Department of Pharmacology, School of Pharmaceutical Sciences, Anhui Medical University, Hefei 230032, China

[c] Department of Endocrinology, Suzhou Ninth People's Hospital, Suzhou Ninth Hospital Affiliated to Soochow University, Suzhou 215200, China

* Corresponding authors

E-mail addresses: fsygkye@163.com(J. Jing); guiyangzhang@ahmu.edu.cn(G. Zhang); 1178336323@qq.com(X. Jiao).

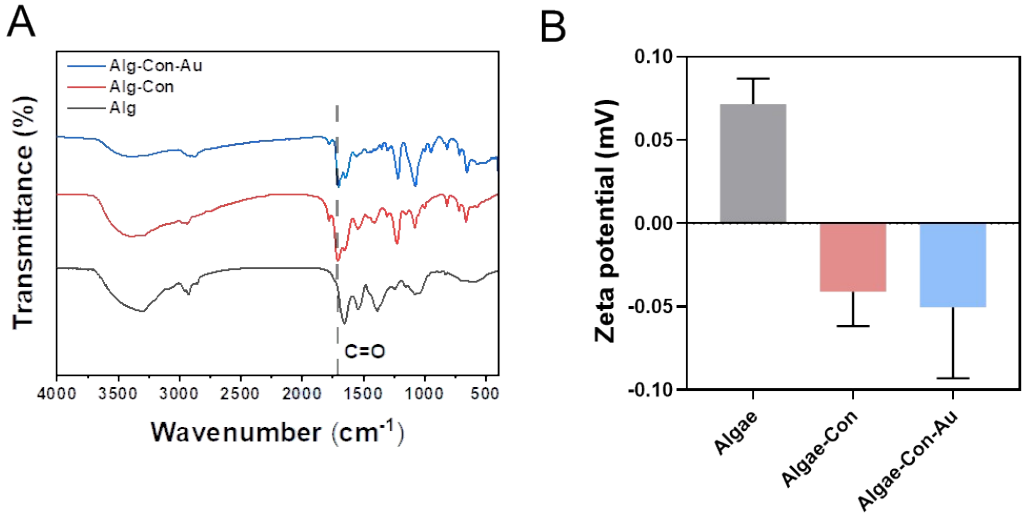

Figure S1. (A) Determination of the ACA complex by Fourier transform infrared spectroscopy. (B) Zeta potential determination of the ACA complex. Data are presented as mean ± standard deviation (n = 3).

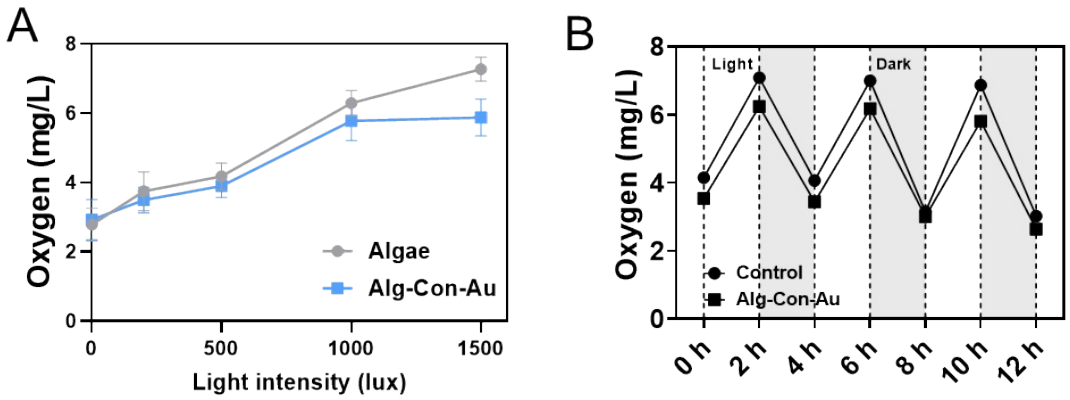

Figure S2. (A) Determination of oxygen production by microalgae under different light intensities. (B) Oxygen content determination of ACA solution at light/dark intervals. Data are presented as mean ± standard deviation (n = 3).

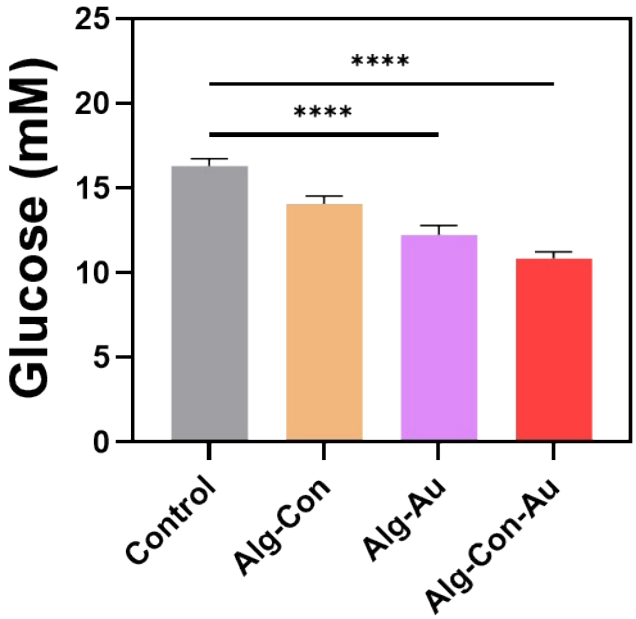

Figure S3. Glucose-lowering effect of ACA and its components determined after 36 h, n = 3. Data are presented as mean ± standard deviation (n = 3), *P < 0.05, **P < 0.01, ***P < 0.001.

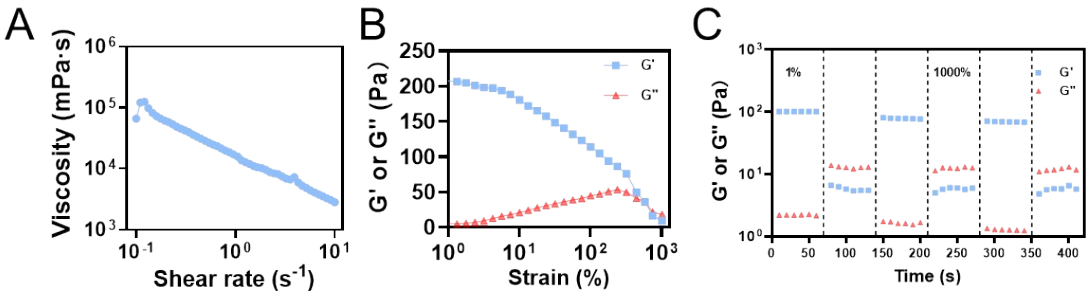

Figure S4. (A) Viscosity/shear rate measurements of gel at 25℃ over a shear rate range of 0.1 to 10 rad/s. (B) Strain amplitude scanning test of gel in the range of 1%-1000% scanning strain. (C) G 'and G "changes between cyclic shear strain 1 and 1000% to verify the self-healing ability of the gel.

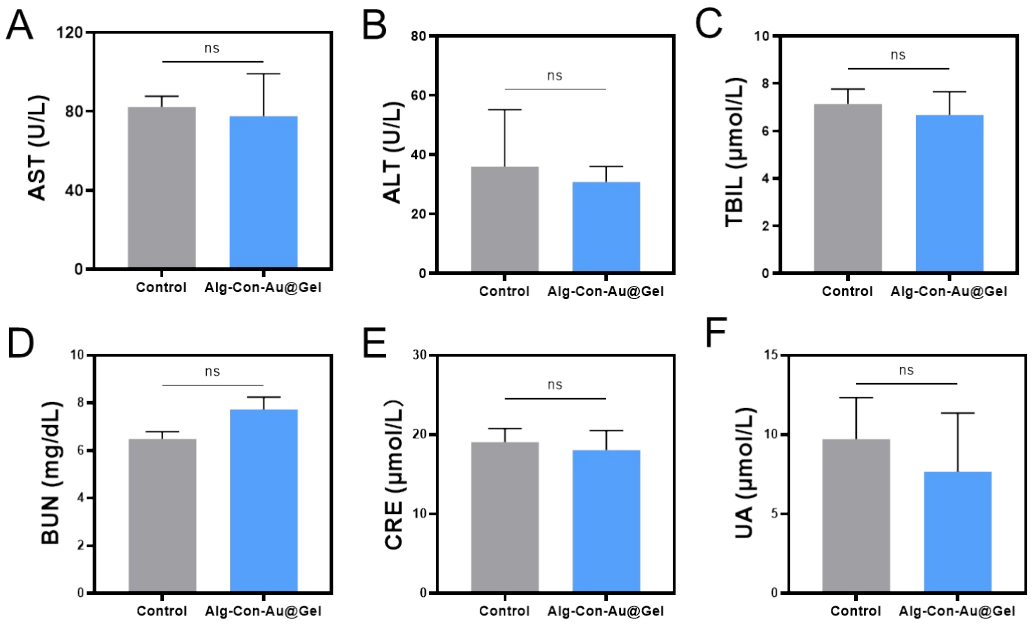

Figure S5. Determination of liver function AST (A), ALT (B), and TBIL (C) and renal function BUN (D), CRE (E), and UA (F) after application of ACA@G gel in the wound of mice.

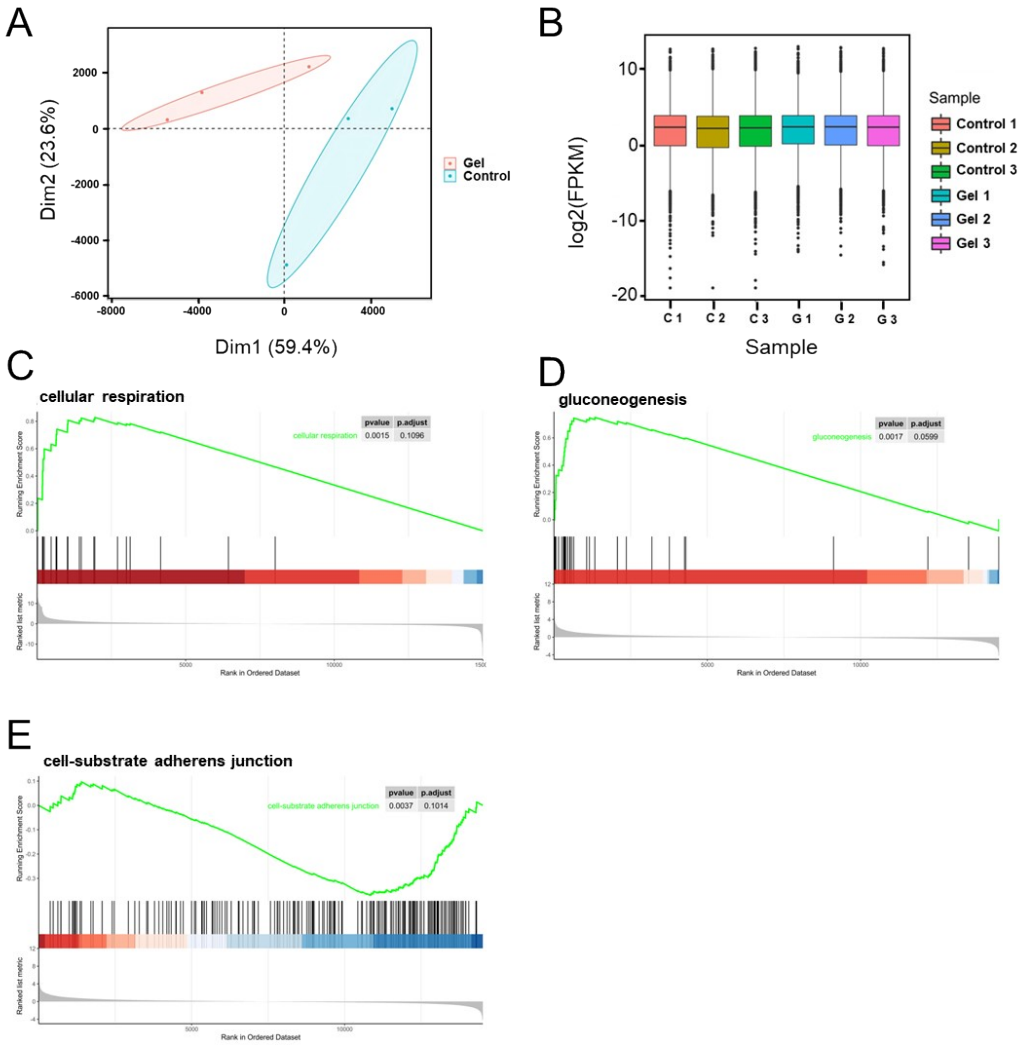

Figure S6. RNA sequencing results after application of ACA@G gel to mouse wounds. (A) Principal component analysis (PCA) of the ACA@G gel and control transcriptomes. (B) Box plots of transcriptomes of ACA@G gel and control groups. (C-E) Gene set enrichment analysis (GSEA).

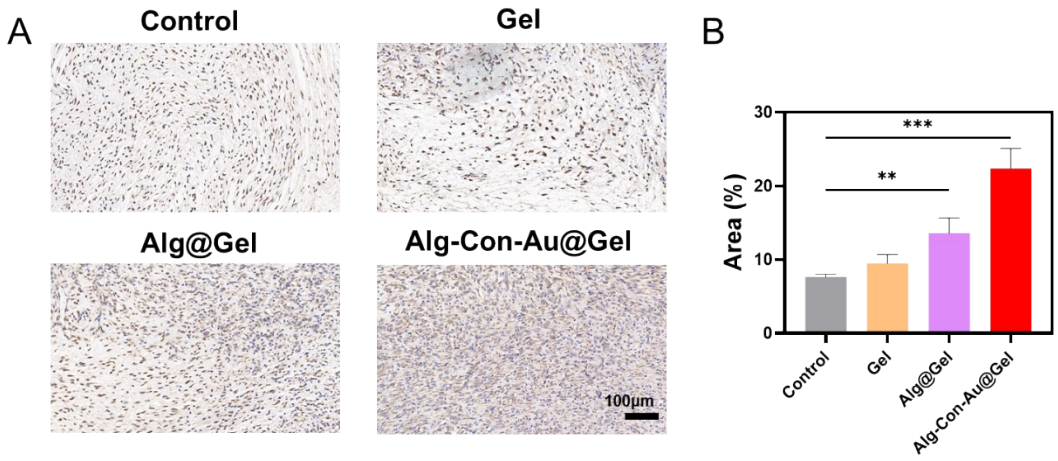

Figure S7. Histological analysis after application of ACA@G gel to diabetic wounds. (A) VEGF immunohistochemical staining of wound tissue on day 6 after surgery, scale bar =100 μm. (B) Quantitative map of VEGF immunohistochemical staining of wound tissue on the 6th day after surgery. Data are presented as mean ± standard deviation (n = 3), *P < 0.05, **P < 0.01, ***P < 0.001.

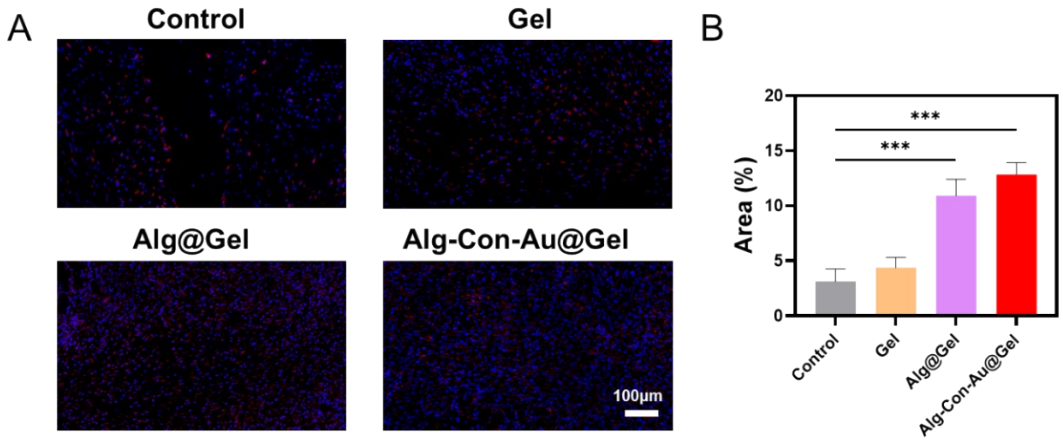

Figure S8. Histological analysis after application of ACA@G gel to diabetic wounds. (A) HIF-1α immunofluorescence staining of wound tissue on POD 6, scale bar = 100 μm. (B) HIF-1α immunofluorescence staining quantitative map of wound tissue on Day 6. Data are presented as mean ± standard deviation (n = 3), *P < 0.05, **P < 0.01, ***P < 0.001.

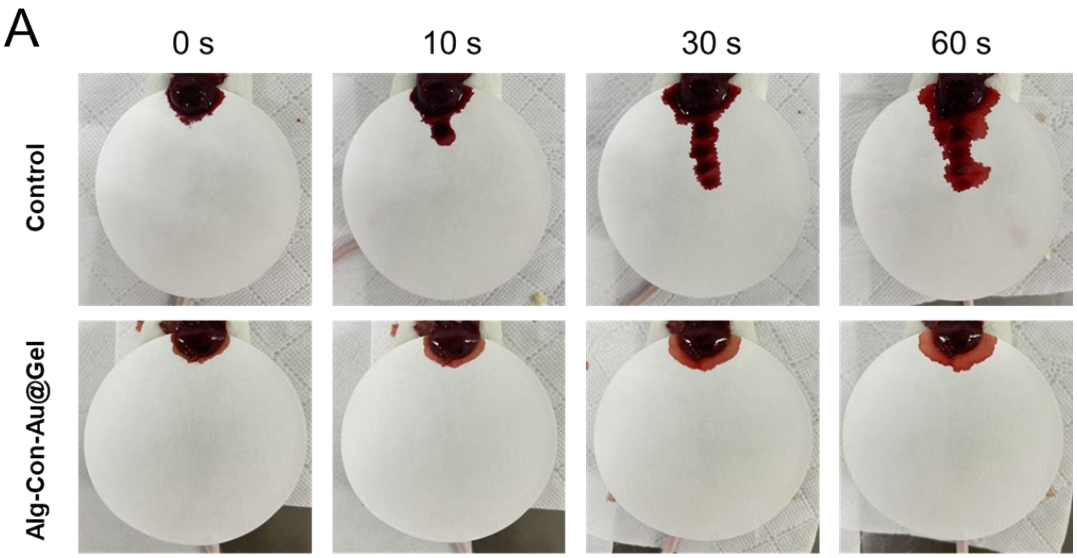
A
0 s
10 s
30 s
60 s
Control
Alg-Con-Au@Gel

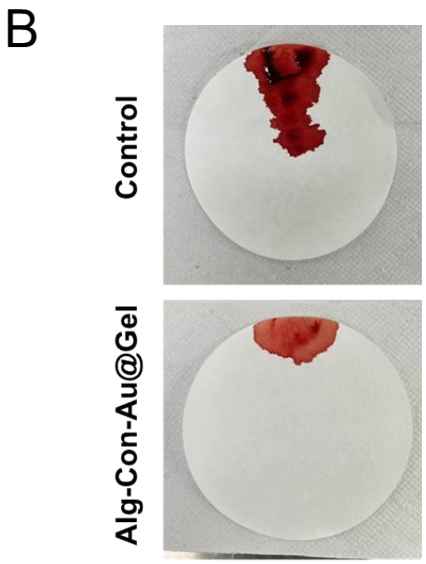
B
Control
Alg-Con-Au@Gel

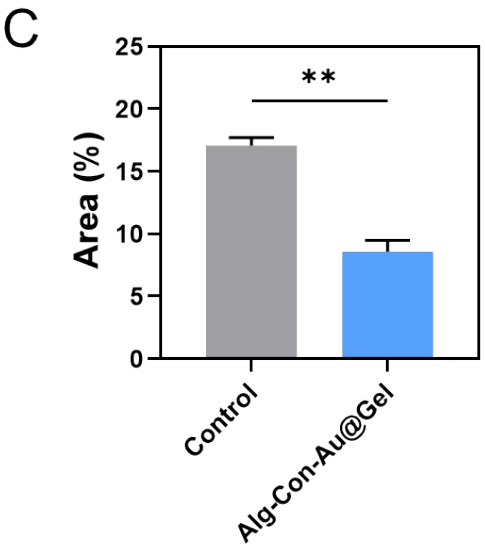
C
Area (%)
25
20
15
10
5
0
**
Control
Alg-Con-Au@Gel

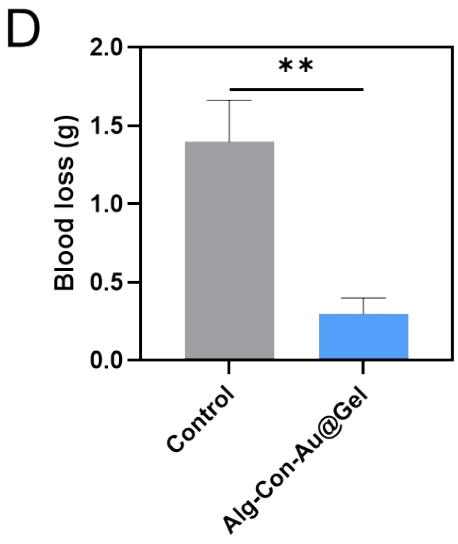
D
Blood loss (g)
2.0
1.5
1.0
0.5
0.0
**
Control
Alg-Con-Au@Gel

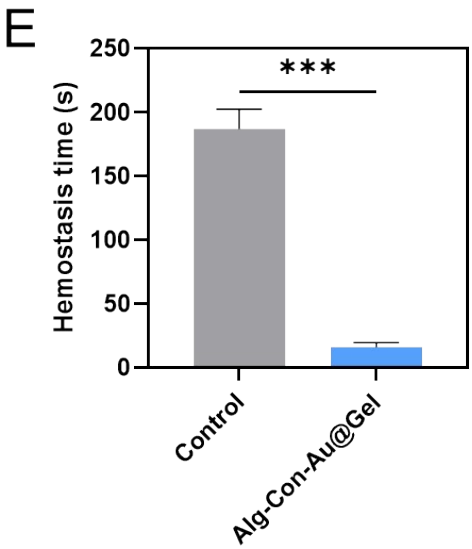
E
Hemostasis time (s)
250
200
150
100
50
0
***
Control
Alg-Con-Au@Gel

Figure S9. Determination of hemostatic Effect of ACA@G gel on Hepatic Hemorrhage. (A) Schematic diagram of hemostasis of hepatic hemorrhage in mice at different time points (0 s, 10 s, 30 s and 60 s) in control group and ACA@G gel group. (B) hemostatic effect diagram and (C) quantitative diagram of control group and ACA@G gel group after 60 s. (D, E) Quantitative analysis of total bleeding volume and hemostasis time of control group and ACA@G gel on hepatic hemorrhage model. Data are presented as mean ± standard deviation (n = 3), *P < 0.05, **P < 0.01, ***P < 0.001.